Spray deposited yttrium incorporated TiO$_2$ photoelectrode for efficient photoelectrocatalytic degradation of organic pollutants☆

N.A. Narewadikar [a], R.S. Pedanekar [a], V.G. Parale [b], H.H. Park [b], K.Y. Rajpure [a, *]

[a] Electrochemical Materials Laboratory, Department of Physics, Shivaji University, Kolhapur, 416004, India
[b] Department of Materials Science and Engineering, Yonsei University, Seoul, 03722, South Korea

ABSTRACT

This work presents result on yttrium-doped titanium dioxide (YTO) thin films using a cost-effective spray pyrolysis technique for the photoelectrocatalytic degradation of phthalic acid (PA) and benzoic acid (BA). The physicochemical properties of YTO thin films were studied using X-ray diffraction, Raman spectroscopy, X-ray photoelectron spectroscopy, field-emission scanning electron microscopy, UV−vis spectroscopy, etc. The obtained results confirm the presence of yttrium in the host lattice. The band bending and flat band positions were studied using Mott−Schottky analysis. The film with 1% doping amount shows the highest degradation efficiency for both the model pollutants compared to TiO$_2$. The stability of 1% YTO film confirms excellent performance analyzed by recycling tests using a UV−vis spectrophotometer. These results highlight the significance of rare earth metal doping in TiO$_2$ for improved photoelectrocatalytic degradation efficiency.

© 2022 Chinese Society of Rare Earths. Published by Elsevier B.V. All rights reserved.

1. Introduction

Photoelectrocatalysis has been fascinating due to its cost-effectiveness and high efficiency in waste water treatment. In heterogeneous photocatalysis, advanced oxidation processes involving ozonation,[1] electrochemical oxidation,[2] sonolysis, and photocatalysis (PC) have been explored to mitigate a variety of organic pollutants present in the environment. Deterioration of organic species using semiconductor photocatalysts has become the most attractive and sustainable strategy to solve environmental pollution. Fujishima and Honda had made rigorous investigations of titanium dioxide (TiO$_2$) due to its ability to split water.[3,4] Among the various metal oxide semiconductors, TiO$_2$ is considered as the most active in wastewater treatment by photocatalytic degradation of pollutants due to the proper position of conduction band edge (E_{CB}) for the facile transfer of electron (e_{CB}^-) to O$_2$.[5] It is a versatile, economical, chemically stable, non-toxic, reliable, and multifunctional material.[6−8] The photocatalytic degradation of dyes in the presence of TiO$_2$ is well known.[9] Anatase TiO$_2$ is the most

photoactive phase due to its enhanced charge carrier mobility and surface hydroxyl groups. The high crystallinity of anatase possesses less surface defects.[10] Apart from its multifunctionality, there are a few limitations in its efficient use: low photonic yield; active only in UV region as band gap is 3.2 eV; in the liquid phase treatment, separation of photocatalysts in the mobile phase is quite complicated.[11,12] Based on literature, there are various preparation methods on titanium based materials which open new perspectives in the field of metal oxide catalysis.[13] Therefore, photocatalysts with higher photocatalytic activities must be economically competitive whose physicochemical properties are excelled by developing TiO$_2$ with various cost-effective synthesis strategies (impurity doping, sensitization, surface modification, etc.).

Doping with rare earth displays enhancement in the catalytic performance and provides strong adsorption capacity.[14] The addition of a small amount of rare earth significantly alters the material properties which is the beauty of rare-earth metal ions. Doping TiO$_2$ with rare earth metal ions could escalate the number of the active sites on the crystal surface as well as generate more oxygen defects. It also mitigates the charge carrier recombination and prolongs the optical response by providing intermediate states in the band gap which contributes to improving photoelectrocatalytic activity.[15,16] Therefore, the research trend in the current area is on
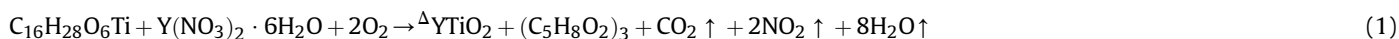
the progression of TiO_2 by tampering with bandgap energy by the addition of defects in the host lattice.[17,18] Rare earth materials like La^{3+}, Ce^{3+}, Eu^{3+},[19] Gd^{3+}, Sm^{3+},[20] Nd^{3+}, etc., have been doped into TiO_2 for photocatalytic applications. It is challenging to step up the condition to incorporate rare-earth ions into the TiO_2 crystal structure due to a difference in ionic radii between the Ti^{4+} and RE^{3+} and the charge imbalance.[21]

The yttrium incorporation inhibits growth and transformation

experiment. The solution was kept for stirring for 10 min and was further used for spraying over the preheated glass substrate/FTO. The synthesized films were labeled as 0.5%YTO, 0.75%YTO, 1%YTO, and 2%YTO, of which the number corresponds to doping concentration. Large-area (10 cm × 10 cm) doped TiO_2 thin film deposited at 450 °C was chosen for testing the degradation of model organic pollutants PA and BA. The pyrolytic reaction that materialized the sample on the surface of FTO at 450 °C is as follows:

$$C_{16}H_{28}O_6Ti + Y(NO_3)_2 \cdot 6H_2O + 2O_2 \xrightarrow{\Delta} YTiO_2 + (C_5H_8O_2)_3 + CO_2 \uparrow + 2NO_2 \uparrow + 8H_2O \uparrow \tag{1}$$

of anatase TiO_2 to rutile phase. Y^{3+} is either located in interstitial positions of the lattice or substituted in Ti^{4+} site or dispersed on the surface of TiO_2 which generates defects in TiO_2. There are two kinds of defects namely, bulk defect and surface defect which have a significant impact on the separation efficiency of electron–hole pairs.[22] Y incorporation decreases band gap energy, hinders crystallite growth and creates the oxygen vacancies. Therefore, due to those reasons Y^{3+} doping enhances the photocatalytic efficiency. Recently, Zhang et al.[23] synthesized yttrium-doped TiO_2 (YTO) by plasma electrolytic oxidation method to improve implant antibacterial properties. Jiang et al.[24] reported YTO hollow microspheres (YTO-HS), which showed enhanced visible-light photocatalytic activity compared to TiO_2-HS for deterioration of methyl orange (MO) by restraining the growth of TiO_2. Niu et al.[25] reported YTO nanoparticles by sol–gel method for evaluation of photocatalytic activity and achieved 99.8% degradation of MO under UV irradiation for 70 min. Zhang et al.[26] studied antibacterial properties against *Staphylococcus aureus* (*S. aureus*) and *Escherichia coli* (*E. coli*) using YTO coating via plasma electrolytic oxidation which was able to boost cell expansion and adhesion. Several methods have been adopted to synthesize YTO films on fluorine-doped tin oxide (FTO). High-quality YTO films were prepared by spray pyrolysis technique which offered a great deal in treating hazardous and toxic chemical wastes into harmless products at ambient temperature with less intermediates.[27]

The aim of this work is to prepare the YTO photoelectrode by a simple approach for the degradation of organic pollutants upon UV irradiation. For this purpose, YTO photoelectrodes were synthesized via a simple and cost-effective spray pyrolysis technique on FTO substrate. Phthalic acid (PA) and benzoic acid (BA) were chosen for systematic investigation of the photoelectrocatalytic performance of the YTO photoelectrodes to facilitate comparison of performance of doped TiO_2. The photodegradation of PA and BA under UV irradiation was checked to evaluate photoelectrocatalytic performance of YTO film. Furthermore, the effects of Y doping concentration on the PEC, structural, morphological properties, and chemical state of spray deposited YTO thin films were also reported.

2. Experimental

2.1. Preparation of pristine TiO_2 and Y^{3+}-doped thin films

The pristine TiO_2 and YTO thin films were prepared by chemical spray pyrolysis method using titanium diisopropoxide bisacetylacetonate (Sigma Aldrich) as Ti source and yttrium nitrate hexahydrate (Y(NO)$_3$.6H$_2$O) as Y precursor. Different concentrations of yttrium (0.5 at%, 0.75 at%, 1 at%, and 2 at%) were added into the ethanolic solution of Ti(OPr)$_2$ (acetylacetonate)$_2$ in separate sets of

Upon spraying the aforementioned solution over the preheated glass/FTO substrates, decomposition of salt into respective oxides with the evaporation of acetylacetone, nitrogen dioxide, and water vapor took place, which resulted in uniform YTO thin films.

2.2. Characterizations of photocatalyst

The photoelectrochemical measurements of the electrodes were studied using the linear sweep voltammetry (LSV) technique (WanAtech automatic battery cycler, Model No. WBCS3000, South korea). YTO film acted as a working electrode while platinum acted as a counter electrode dipped in electrolyte with electrolyte area (1 cm^2) exposure to UV light (20 mW/cm^2), separated by 0.5 cm apart. An aqueous solution of 0.1 mol/L NaOH was used as an electrolyte to improve the reaction rate. The structural data were recorded by a Bruker X-ray diffractometer (Model D8 advances, Germany) with Cu Kα radiation of wavelength of 0.15418 nm. The surface morphologies of TiO_2 and YTO films were observed by a field emission scanning electron microscope (FESEM-JEOL JSM 7001F, Japan) operated at 15 kV with a thin layer of gold sputter-coating before analysis. Energy dispersive X-ray analysis (EDX) was used to determine chemical composition. The chemical states of TiO_2 and YTO films were examined using an X-ray photoelectron spectrometer (Model: Kα, Thermo Scientific Inc., U.K) at room temperature. The detailed chemical structure of the samples was studied using micro-Raman spectroscopy (Renishaw INVIA0120-02, UK). An excitation wavelength of 532 nm at a power level of 1% with a resolution of 0.5 cm^{-1} was used to record Raman spectra. The optical properties of the thin films as well as model pollutants were recorded using a UV–vis 1800 spectrophotometer (Shimadzu, Japan).

3. Results and discussion

3.1. Photoelectrocatalytic performance of the catalyst

Fig. 1(a) displays the photocurrent density–voltage curves obtained with a linear sweep voltammetry technique. The PEC performance of the pristine TiO_2 and YTO films was measured with a two-electrode system under UV illumination. The photocurrent density of YTO films increased with dopant concentration (0.5%–2%) but later decreased for higher concentrations.

The 1%YTO film showed the best photocurrent density (1.28 mA/cm^2) toward the reaction recorded in the range of an applied potential window (−1 to 1 V) compared to pristine TiO_2 film. 2%YTO film exhibited lower photocurrent density due to more number of defects which act as recombination centers for depletion of photocurrent.
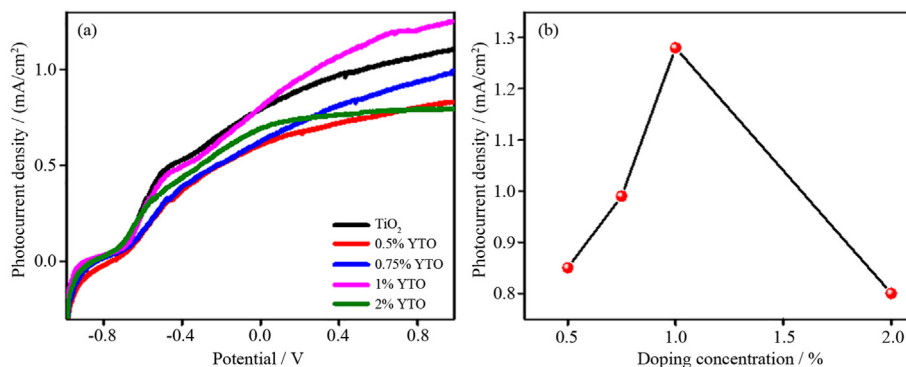
N.A. Narewadikar, R.S. Pedanekar, V.G. Parale et al.

Fig. 1. (a) Plots of photocurrent density against the potential of pristine and doped TiO_2 thin films; (b) Variation of photocurrent density with dopant concentration (0.5%−2%).
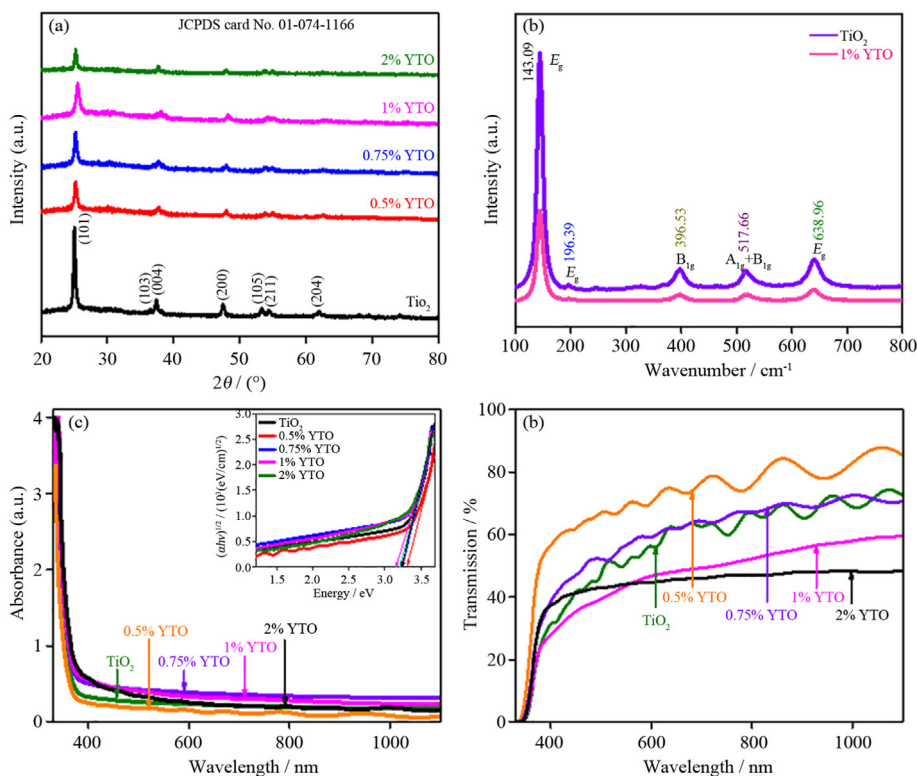

Fig. 2. (a) XRD patterns of pristine TiO_2 and YTO films; (b) Raman spectra of pristine TiO_2 and YTO films; Absorbance (c) and transmittance (d) spectra of both pristine TiO_2 and YTO films.

This means that charge carrier separation and transport were more effective in the 1%YTO electrode than other films. The performance of photocurrent density with variant dopant concentration is displayed in Fig. 1(b). Therefore, 1% is the optimal doping concentration of YTO film used for large-area thin film deposition for degradation experiment.

3.2. Structural and optical studies

X-ray diffraction (XRD) analysis revealed the crystallographic structures of the pristine TiO_2 and YTO films (Fig. 2(a)). The XRD profiles of TiO_2 and YTO films confirm a tetragonal anatase phase with the most prominent orientation along the (101) plane (JCPDS No. 01-074-1166). The intensity of the (101) plane of YTO films is decreased as compared to pristine TiO_2 film due to the generation of defect states. The intensity of the diffraction peaks decreased with an increase in doping concentration. In this case, no peak is observed for yttrium which indicated the proper doping amount of yttrium in TiO_2 lattice.[28] Y incorporation in host TiO_2 showed a gradiation trend in crystallite size (21−42 nm). The smaller crystallite size for 1%YTO film reveals that Y^{3+} ions pile up at the grain junction, which inhibits the crystallite growth due to a mismatch of ionic radius.[29]

Fig. 2(b) shows Raman spectra of pristine TiO_2 and 1%YTO thin films. Anatase TiO_2 has six Raman-active modes $(A_{1g} + 2B_{1g} + 3E_g)$.[30] These six characteristics of active modes are attributed to vibrational modes with distinct peaks at 143.43, 195.5, 396.89, 516.21, and 639.66 cm^{-1}, corresponding to the anatase phase. Y incorporation in host TiO_2 induced a small shift and reduced peak intensity with higher content of Y^{3+}, which is ascribed to the extension of the crystal lattice by generating defects and oxygen vacancies.[31] The observational data from Raman and

Table 1
Band gap values of pristine and doped TiO$_2$.

Samples	Thickness (μm)	Band gap energy (eV)
TiO$_2$	1.912	3.23
0.5%YTO	1.874	3.3
0.75%YTO	2.014	3.24
1%YTO	2.109	3.15
2%YTO	2.148	3.2

XRD analysis confirmed the incorporation of Y^{3+} ions in the host TiO$_2$ lattice.

The optical performance of pristine TiO$_2$ and YTO films is displayed in Fig. 2(c and d). The absorption edge shifts to a slightly higher wavelength side with increasing doping concentration. Fig. 2(d) shows the oscillating nature of transmittance which is due to the interference effect. This wavy nature gets flattened with increasing doping concentration due to increased scattering effect. Inset shows the band gap values of the YTO film which were calculated by using Tauc's formula[32] and are listed in Table 1. It is observed that absorption is thickness-dependent. The increase in relative transmittance in the 0.5% doping may be attributed to the possibility of replacement of Ti or O by Y in lattice thereby reducing defect states. Decrease in relative transmittance with respect to Y doping concentration might be due to increase in film thickness thereby increasing defect states and scattering.

3.3. XPS

The chemical bonding states and binding energy of pristine TiO$_2$ and YTO films were examined by XPS spectra. The XPS verifies the successful loading of Y into the host TiO$_2$ lattice. Fig. 3(a) shows the

XPS survey scan spectrum of the YTO film at 1% dopant concentration along with photoemissions and Auger peaks ascribed to Y 3d, Ti 2p, C 1s, and O 1s elements, respectively. The peak observed at binding energy 284.4eV was attributed to hydrocarbon deposited over the film as all the signals while testing samples were calibrated with respect to carbon signal.[33,34] Fig. 3(b) shows Ti 2p level narrow scan XPS spectrum which was observed as doublets located at 458.5 and 464.3 eV were ascribed to the Ti 2p$_{3/2}$ and Ti 2p$_{1/2}$ states due to spin−orbit splitting characteristic which confirms the presence of Ti.[18] It is observed that there is a slight shift of the peak to lower binding energy and an increase in peak intensity of YTO film than that of pristine TiO$_2$, which is a signature of presence of Y and charge imbalance. The peak-to-peak separation of Ti 2p peaks is 5.72 eV, showing the Ti−O bonding in TiO$_2$ for YTO film, where peaks are ascribed to the presence of Ti^{4+} state.[35] Fig. 3(c) depicts the Y 3d level narrow scan XPS spectrum of 1% YTO film where two peaks observed at 157.8 and 159.7 eV correspond to Y 3d$_{5/2}$ and Y 3d$_{3/2}$ states, which verifies the presence of Y^{3+} in the TiO$_2$, while the third peak appearing at 156 eV corresponds to Y 3d$_{5/2}$ state which is the characteristic peak of Y$_2$O$_3$.[27,36] The mismatch arises from difference in Y−O bond lengths between Y$_2$O$_3$ and YTO crystal lattices.[37] Fig. 3(d) shows the narrow scan O 1s XPS spectrum. The O 1s peak is observed at 529.8 eV, assigned to the lattice oxygen in O$^{2−}$ form, bound directly to 2 Ti atoms, i.e., the, peaks shift at lower B.E (531.14 and 529.56 eV) were assigned to the bonding energies of the Y−O and Ti−O bonds which manifest the presence of oxygen vacancies in the 1%YTO film.[24,38] The other peak is observed at 531.2 eV which is due to surface hydroxyl group. The photoinduced holes can attack the surface hydroxyl groups and produce OH radicals with high oxidation capability.[39] It is reported that doping Y^{3+} in Ti^{4+} decreases one electron, which would be compensated by forming oxygen vacancies. Therefore, Ti^{3+} state
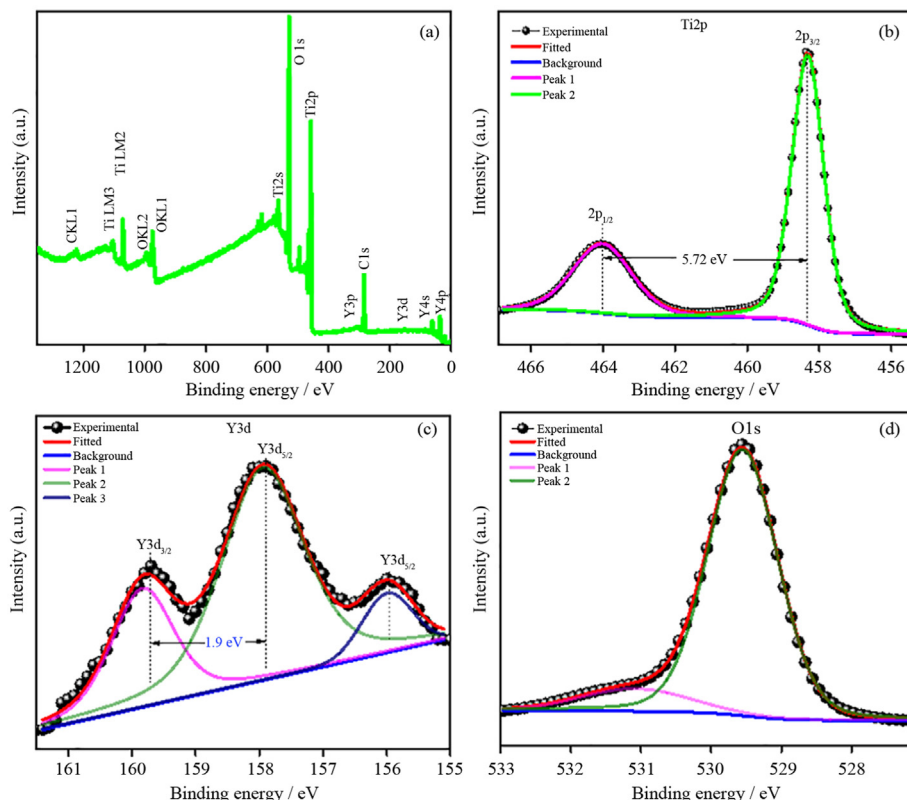

Fig. 3. (a) Survey scan XPS spectrum of YTO film; Narrow scan XPS spectra of Ti 2p (b), Y 3d (c), and O 1s (d).
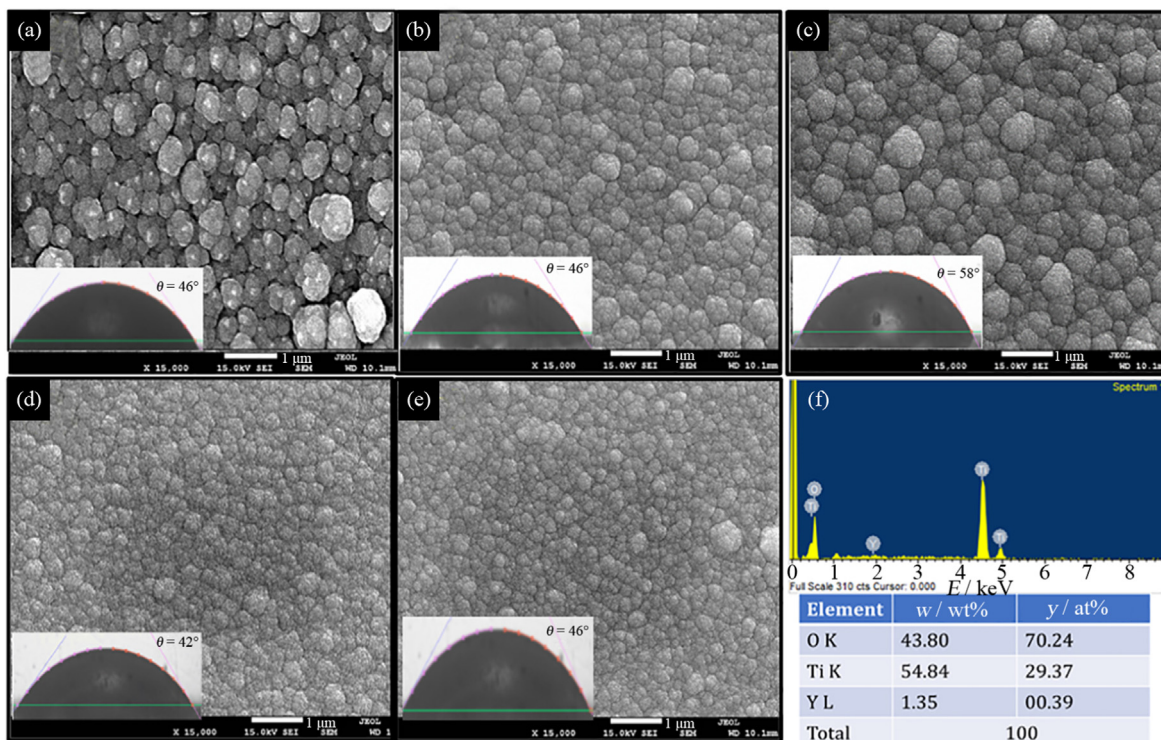
Fig. 4. FESEM images of Y-doped TiO$_2$ at different dopant concentrations: (a) TiO$_2$; (b) 0.5%YTO; (c) 0.75%YTO; (d) 1%YTO; (e) 2%YTO; (f) EDAX spectrum of 1%YTO film for elemental composition analysis.

existed in the Y doped TiO$_2$ in which oxygen vacancy defects were generated.[40]

3.4. Morphological, elemental analysis, and surface wettability study

Fig. 4(a−e) show morphological study of pristine TiO$_2$ and YTO films. It is examined that the surface of 1%YTO film is closely packed with rough surface and pebble shaped morphology where adsorption is comparatively higher than that in other films. Therefore, 1%YTO film is further used for photoelectrocatalytic study for better degradation performance. The insets in Fig. 4 show the contact angle of each sample with different concentrations. It varies with respect to dopant concentrations (42°−58°). The elemental composition profile of 1%YTO film is shown in Fig. 4(f).

The atomic ratio of Y/Ti is 0.0102, which represents a minimal amount of Y present in the film.

3.5. Mott−Schottky (MS) analysis

MS analysis was carried out using three electrode systems with 0.1 mol/L NaOH as electrolyte applied during experiment. The flat band potential (U_{fb}) of pristine TiO$_2$ and 1%YTO film was obtained by extrapolation of the Mott−Schottky plots (C_{sc}^{-2} vs. U) (Fig. 5(a)) using the equation.[41] It provides the information of charge transport across the junction of photoelectrode and electrolyte. The slope of this curve gives carrier density which is higher for 1%YTO film (5.66 × 10^{11} cm^4/F^{-2}) than that for pristine TiO$_2$ (4.42 × 10^{11} cm^4/F^2). The value of U_{fb} of 1%YTO was estimated to be −0.8 V/SCE which is more negative than that of pristine TiO$_2$. The negative value of flat band potential indicates that it is n-type
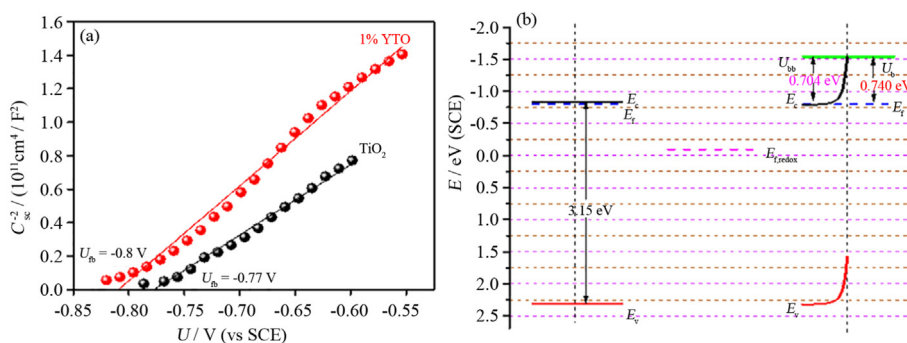

Fig. 5. (a) Mott−Schottky plots for pristine TiO$_2$ and 1%YTO film; (b) Flat band and band bending positions of 1%YTO/0.1 mol/L NaOH/Pt.

N.A. Narewadikar, R.S. Pedanekar, V.G. Parale et al.

material which reduced exciton recombination to facilitate better charge separation in PEC reaction.[42]

$$\frac{1}{C_{SC}^2} = \frac{2}{N_D \ \varepsilon_0 \varepsilon_{TiO_2} e} \left(E - E_{fb} - \frac{k_B T}{e} \right) \qquad (2)$$

where C is the space charge capacitance, E the external applied potential, E_{fb} the flat band potential, N_D the donar density, ϵ_0 and ϵ_{TiO2} are the permittivity of the free space and semiconductor, T is the operating temperature, and k_B is the Boltzmann constant.
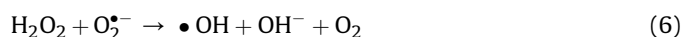
Fig. 5(b) shows flat band position and band bending of 1%YTO/ 0.1 mol/L NaOH/Pt system. The conduction band edge (E_c) lies above the flat band potential by 0.04 eV at −0.83 eV/SCE. The amount of band bending potential (U_{bb}) in case of 1%YTO film is 0.704 eV which is the difference between flat band potential of semiconductor and redox potential of an electrolyte. The barrier height (U_b) was also calculated and is shown in Fig. 5(b).

3.6. EIS and photocurrent response measurement

The interfacial charge transfer kinetics of pristine TiO_2 and 1% YTO were carried out by transient photocurrent response over time measured at +1 V potential with chopped illumination at a rate of 20 s exposure followed by 20 s no illumination for UV light as shown in Fig. 6(a). The sharp spikes in the photocurrent during ON/ OFF illumination for both the cases indicate fast transport of photogenerated electrons at electrode−electrolyte interface. The photocurrent density of 1%YTO film was higher than that of pristine TiO_2 which can be confirmed by a charge transfer resistance measured by the electrochemical impedance spectroscopy (EIS). The lesser the value of charge transfer resistance is, the higher the photocurrent response is. The charge transfer and recombination dynamics at photoelectrode interface were studied by EIS technique.[43] Photoresponse curve indicates that yttrium incorporation in TiO_2 can promote the separation and transfer of the charge carriers effectively and suppress the recombination of photogenerated carrier efficiency at the interface of 1%YTO.[44] Generally, the charge transfer resistance is shown by the radius of curvature in EIS spectra. The smaller semicircle diameter in EIS implies the higher charge transfer efficiency and better electron conductivity. Fig. 6(b) shows Nyquist plots of pristine TiO_2 and 1%YTO film measured in dark and light, respectively. The characteristic peak represented by a smaller semicircle indicates the high-frequency region in the Nyquist plots. The smaller semicircle of 1%YTO indicates the enhancement of the charge separation efficiency of 1%YTO film than that of pristine TiO_2 which indicates greater photodegradation activity. The result is consistent with the transient photocurrent response.

3.7. Photoelectrocatalytic activity and photoelectrochemical (PEC) measurements

The mechanism of the photoelectrocatalytic process upon incidence of light on semiconductors was studied elsewhere,[45] where charge carriers are generated upon incidence of a photon over a semiconductor. The PEC reaction mainly occurred on the surface of photoelectrode. The adsorption reaction of the YTO electrode surface will be an essential task in the deterioration of organic species (PA and BA). The active species (h^+, $\cdot O_2^-$ and $\cdot OH$) generated in the PEC reaction play a crucial role in the degradation process, as expressed by the equations.[46]

$$h^+ + H_2O \rightarrow H^+ + \bullet OH \qquad (3)$$

$$e^- + O_2 \rightarrow O_2^{\bullet-} \qquad (4)$$

$$e^- + O_2 + 2H^+ \rightarrow H_2O_2 \qquad (5)$$

$$H_2O_2 + O_2^{\bullet-} \rightarrow \bullet OH + OH^- + O_2 \qquad (6)$$

During this process, electrons and holes migrate to the respective surfaces to react with adsorbed species after applying external bias potential, increasing photoelectrocatalytic performance. During photoelectrocatalytic degradation process, a large-area 1%YTO film was mounted on a reactor set up as a photoanode along with a gasket to maintain the pollutant flow in a proper channel. The pollutants (PA and BA) are allowed to pass separately through reactor (at pH = 5) in the dark for 30 min for sufficient adsorption using a peristaltic pump. After adsorption continued, the external bias of 1.5 V was applied across the electrodes to hinder the charge carrier recombination and increase the degradation rate and the backside of the photoelectrode was illuminated using UV irradiation to promote redox reaction. After a certain interval of time t, aliquots (PA and BA) under photoelectrocatalytic treatment were taken from the reactor to quantify pollutant concentration. The Y^{3+} ions trap the free electrons, which then react with the absorbed O_2 to form reactive $\cdot O_2^-$ as well as $\cdot OH$, capable of decomposing organic dyes into harmless materials such as CO_2 and H_2O. Fig. 7(a) displays extinction spectra of PA collected at various time intervals during photoelectrocatalysis. The extinction peak intensity for both pollutants decreases with increasing reaction time due to degradation over a period of time as shown in Fig. 7(a, c). The degradation kinetics of the catalysts was also studied. The electrostatic force between the organic species and the catalyst is responsible for the adsorption followed by photodegradation. The oxidative degradation efficiency and decomposition rate constants were
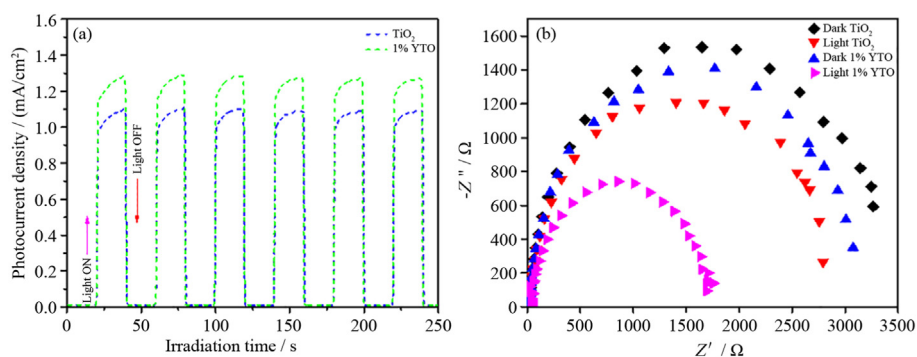

Fig. 6. (a) Transient photocurrent response for the pristine TiO_2 and 1%YTO film under dark and UV light irradiation; (b) Nyquist plots of the pristine TiO_2 and 1%YTO film.
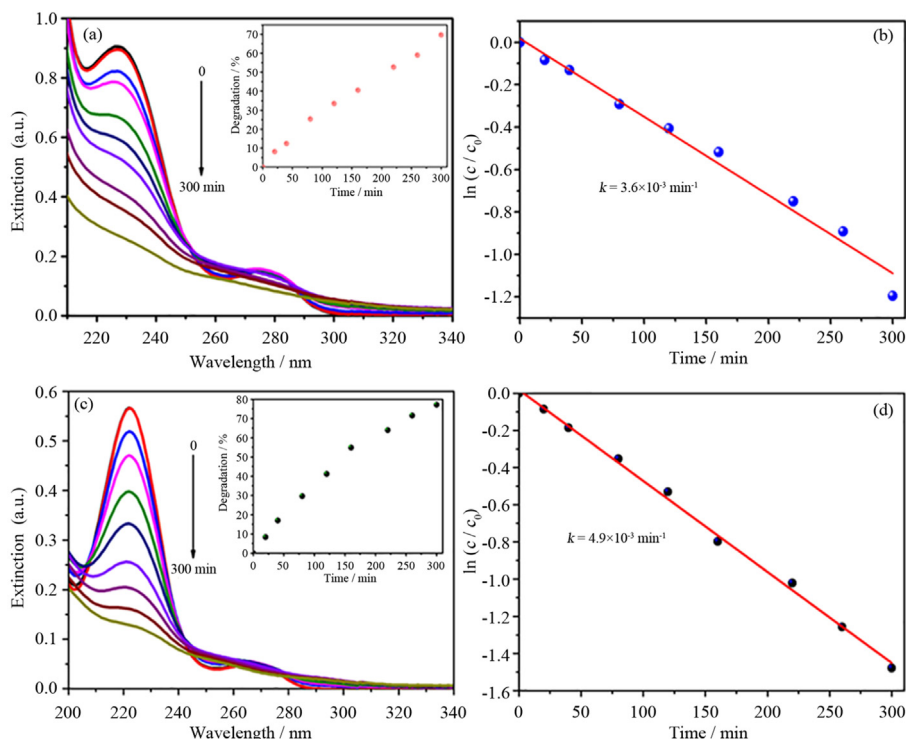
Fig. 7. (a) Extinction spectra of PA with the function of wavelength where inset shows degradation performance varies with respect to time; (b) Logarithmic plot of c/c_0, which is a function of time; (c) Extinction spectra of BA, which is a function of wavelength where inset shows degradation efficiency with respect to time; (d) Logarithmic plot of c/c_0, which is a function of time.

calculated using Langmuir-Hinselwood expression reported earlier.[9]

The insets of Fig. 7(a, c) show the degradation efficiencies of both PA and BA pollutants using a 1%YTO electrode in 300 min. The kinetics of degradation of PA and BA pollutants were studied and monitored, as shown in Fig. 7(b, d). The slope of these plots gives the rate constant (k) to be 3.6×10^{-3} min^{-1} for PA and 4.9×10^{-3} min^{-1} for BA, which is 1.5 times higher than pristine TiO$_2$. The value of R^2 or coefficient of determination (COD) is be 0.989 for PA and 0.993 for BA which revealed that the degradation rate in both cases follows the first-order kinetics concerning the radiation absorption rate. A superior photoelectrocatalytic degradation capability of YTO film was observed due to improved light absorption behavior of the TiO$_2$ film towards redshift, and 1%YTO exhibits a smaller crystallite size than the rest of the films. The rate constant values of 1%YTO film for PA and BA pollutants are higher than that of pristine TiO$_2$ which are 2.9×10^{-3} min^{-1} and 3.3×10^{-3} min^{-1}, respectively. In comparison to the representative TiO$_2$-based photocatalysts, yttrium-incorporated TiO$_2$ photoelectrode showed better UV-light-driven photoelectrocatalytic activity (Table 2).

The photostability and reusability of the 1%YTO photocatalyst are important tasks for degradation. To test the reusability of 1%
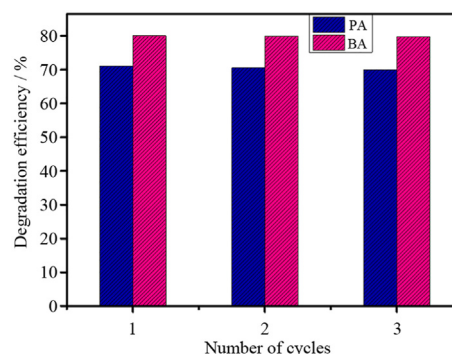

Fig. 8. Cyclic photostability of 1%YTO film over PA and BA.

YTO photocatalyst, recycled PEC degradation of PA and BA (250 mL) was performed over 1%YTO photoelectrode under UV illumination. The same experiment was repeated twice with fresh organic species. Fig. 8 displays the degradation efficiency (%) with the number of degradation cycles. 1%YTO film exhibits the best PEC stability even after 3 cycles.

Table 2
A comparison of dye degradation by the YTO composite with previously reported TiO$_2$-based photocatalysts.

Sr No.	Catalysts	Efficiency (%)	Organic pollutants	Ref.
1	N−TiO$_2$	64%	Rh B dye	[47]
2	Ni−TiO$_2$	78%	Ibuprofen	[48]
3	Y−TiO$_2$ hollow sphere	~70%	Methyl orange (MO)	[24]
4	Ag/TiO$_2$-DLE	78.85%	MO	[49]
5	Y−TiO$_2$	71%	PA	Present work
		79%	BA	

The photoelectrocatalytic degradation mechanism pathway of PA and BA using the YTO film is discussed here since pristine TiO_2 showed low photocatalytic activity. Incident photon having energy greater than or equal to band gap energy is absorbed by YTO thin film which creates excitons. The generated excitons are separated by applying external bias. The electrons in the valence band (VB) jump into the CB by leaving behind holes in the VB which interacts with Y^{3+} ion and move towards counter electrode which opened the way for the reduction process to form superoxide anion. The holes in the VB tend to form highly reactive OH radical or directly oxidize organic species. Both $\cdot OH$ and O_2^- react with organic pollutants to deteriorate the pollutants into harmless byproducts. The detailed degradation mechanism pathway along with their byproduct of PA and BA is discussed in literature .[50–52] Hence, yttrium doping in anatase TiO_2 contributed to the excellent photoelectocatalytic property.

4. Conclusions

YTO photoelectrodes were successfully deposited via a simple spray pyrolysis approach. Compared with pristine TiO_2, the film with 1% Y doping exhibits an absorption shift towards higher wavelength, suppressing the electron−hole pair recombination. The charge compensation in YTO was done by forming oxygen vacancy, which was analyzed by XPS. 1%YTO electrode exhibits amelioration of photoelectrocatalytic performance of PA and BA compared to pristine TiO_2 under UV illumination. The flat band potentials of pristine TiO_2 and YTO thin film respectively are −0.77 and −0.8 V/SCE measured with the help of MS plots. Conclusively, incorporating Y^{3+} ions into TiO_2 results in better performance of optical properties of TiO_2, which is a better candidate as a photoelectrode for photoelectrocatalytic degradation of organic pollutants.

Declaration of competing interest

The authors declare that they have no conflict of interest.

Acknowledgments

References

1. Zeng Y, Chen D, Chen T, Cai M, Zhang Q, Xie Z, et al. Study on heterogeneous photocatalytic ozonation degradation of ciprofloxacin by TiO_2/carbon dots: kinetic, mechanism and pathway investigation. *Chemosphere*. 2019;227:198.
2. Xie R, Meng XY, Sun PZ, Niu JF, Jiang WJ, Bottomley L, et al. Electrochemical oxidation of ofloxacin using a TiO_2-based SnO_2-Sb/polytetrafluoroethylene resin-PbO_2 electrode: reaction kinetics and mass transfer impact. *Appl Catal, B*. 2017;203:515.
3. Fujishima A, Zhang X, Tryk D. TiO_2 photocatalysis and related surface phenomena. *Surf Sci Rep*. 2008;63:515.
4. Lan Y, Lu Y, Ren Z. Mini review on photocatalysis of titanium dioxide nanoparticles and their solar applications. *Nano Energy*. 2013;2:1031.
5. Park H, Park Y, Kim W, Choi W. Surface modification of TiO_2 photocatalyst for environmental applications. *J Photochem Photobiol, C*. 2013;15:1.
6. Reszczyńska J, Grzyb T, Sobczak JW, Lisowski W, Gazda M, Ohtani B, et al. Visible light activity of rare earth metal doped (Er^{3+}, Yb^{3+} or Er^{3+}/Yb^{3+}) titania photocatalysts. *Appl Catal, B*. 2015;163:40.
7. Parale VG, Kim T, Phadtare VD, Yadav HM, Park H-H. Enhanced photocatalytic activity of a mesoporous TiO_2 aerogel decorated onto three-dimensional carbon foam. *J Mol Liq*. 2019;277:424.
8. Zhou W, Li W, Wang J-Q, Qu Y, Yang Y, Xie Y, et al. Ordered mesoporous black TiO_2 as highly efficient hydrogen evolution photocatalyst. *J Am Chem Soc*. 2014;136:9280.
9. Ma F, Yang Q, Wang Z, Liu Y, Xin J, Zhang J, et al. Enhanced visible-light photocatalytic activity and photostability of Ag_3PO_4/Bi_2WO_6 heterostructures toward organic pollutant degradation and plasmonic Z-scheme mechanism. *RSC Adv*. 2018;8:15853.
10. Zhou W, Sun F, Pan K, Tian G, Jiang B, Ren Z, et al. Well-ordered large-pore mesoporous anatase TiO_2 with remarkably high thermal stability and improved crystallinity: preparation, characterization, and photocatalytic performance. *Adv Funct Mater*. 2011;21:1922.
11. Silva CG, Faria JL. Photocatalytic oxidation of benzene derivatives in aqueous suspensions: synergic effect induced by the introduction of carbon nanotubes in a TiO_2 matrix. *Appl Catal, B*. 2010;101:81.
12. Li Z, Li H, Wang S, Yang F, Zhou W. Mesoporous black $TiO_2/MoS_2/Cu_2S$ hierarchical tandem heterojunctions toward optimized photothermal-photocatalytic fuel production. *Chem Eng J*. 2022;427:131830.
13. Reghunath S, Pinheiro D, Kr SD. A review of hierarchical nanostructures of TiO_2: advances and applications. *Appl Surf Sci Adv*. 2021;3:100063.
14. Zhao L, Li G, Li F, Yao M. Enhanced visible light photoactivity of TiO_2/SnO_2 films by tridoping with Y/F/Ag ions. *J Rare Earths*. 2022;40:616.
15. Liu D, Zhou J, Wang J, Tian R, Li X, Nie E, et al. Enhanced visible light photoelectrocatalytic degradation of organic contaminants by F and Sn co-doped TiO_2 photoelectrode. *Chem Eng J*. 2018;344:332.
16. Zheng F, Dong F, Zhou L, Yu J, Luo X, Zhang X, et al. Cerium and carbon-sulfur codoped mesoporous TiO_2 nanocomposites for boosting visible light photocatalytic activity. *J Rare Earths*. 2023;41(4):539.
17. M PK, G.A SJ, G T, A S, J S. Rare earth doped semiconductor nanomaterials and its photocatalytic and antimicrobial activities. *J Environ Chem Eng*. 2018;6:3907.
18. Prabakaran S, Nisha KD, Harish S, Archana J, Navaneethan M. Yttrium incorporated TiO_2/rGO nanocomposites as an efficient charge transfer layer with enhanced mobility and electrical conductivity. *J Alloys Compd*. 2021;885:160936.
19. Li S, Yang Y, Su Q, Liu X, Zhao H, Zhao Z, et al. Synthesis and photocatalytic activity of transition metal and rare earth element co-doped TiO_2 nano particles. *Mater Lett*. 2019;252:123.
20. Arévalo-Pérez JC, de la Cruz-Romero D, Cordero-García A, Lobato-García CE, Aguilar-Elguezabal A, Torres-Torres JG. Photodegradation of 17 α-methyltestosterone using TiO_2-Gd^{3+} and TiO_2-Sm^{3+} photocatalysts and simulated solar radiation as an activation source. *Chemosphere*. 2020;249:126497.
21. Choi J, Park H, Hoffmann MR. Effects of single metal-ion doping on the visible-light photoreactivity of TiO_2. *J Phys Chem C*. 2010;114:783.
22. Li Z, Wang S, Wu J, Zhou W. Recent progress in defective TiO_2 photocatalysts for energy and environmental applications. *Renew Sustain Energy Rev*. 2022;156:111980.
23. Zhang B, Li B, Gao S, Li Y, Cao R, Cheng J, et al. Y-doped TiO_2 coating with superior bioactivity and antibacterial property prepared via plasma electrolytic oxidation. *Mater Des*. 2020;192:108758.
24. Jiang X, Gao Y, Li C, You F, Yao J, Ji Y, et al. Preparation of hollow yttrium-doped TiO_2 microspheres with enhanced visible-light photocatalytic activity. *Mater Res Express*. 2019;6:065510.
25. Niu X, Li S, Chu H, Zhou J. Preparation, characterization of Y^{3+}-doped TiO_2 nanoparticles and their photocatalytic activities for methyl orange degradation. *J Rare Earths*. 2011;29:225.
26. Zhang B, Li B, Gao S, Li Y, Cao R, Cheng J, et al. Y-doped TiO_2 coating with superior bioactivity and antibacterial property prepared via plasma electrolytic oxidation. *Mater Des*. 2020;192:108758.
27. Zhang W, Wang K, Zhu S, Li Y, Wang F, He H. Yttrium-doped TiO_2 films prepared by means of DC reactive magnetron sputtering. *Chem Eng J*. 2009;155:83.
28. Li Y, Guo Y, Li Y, Zhou X. Fabrication of Cd-doped TiO_2 nanorod arrays and photovoltaic property in perovskite solar cell. *Electrochim Acta*. 2016;200:29.
29. Zhang Q, Fu Y, Wu Y, Zhang Y-N, Zuo T. Low-cost Y-doped TiO_2 nanosheets film with highly reactive {001} facets from CRT waste and enhanced photocatalytic removal of Cr(VI) and methyl orange. *ACS Sustainable Chem Eng*. 2016;4:1794.
30. Pal M, Pal U, Jiménez JMGY, Pérez-Rodríguez F. Effects of crystallization and dopant concentration on the emission behavior of TiO_2:Eu nanophosphors. *Nanoscale Res Lett*. 2012;7:1.
31. Khan S, Ikari H, Suzuki N, Nakata K, Terashima C, Fujishima A, et al. One-pot synthesis of anatase, rutile-decorated hydrogen titanate nanorods by yttrium doping for solar H_2 production. *ACS Omega*. 2020;5:23081.
32. Rajpure KY, Lokhande CD, Bhosale CH. A comparative study of the properties of spray-deposited Sb_2Se_3 thin films prepared from aqueous and nonaqueous media. *Mater Res Bull*. 1999;34:1079.
33. Martín VC-S, Morales-Luna M, García-Tinoco PE, Pérez-González M, Arvizu MA, Crotte-Ledesma H, et al. Chromogenic MoO_3 thin films: thermo-, photo-, and electrochromic response to working pressure variation in rf reactive magnetron sputtering. *J Mater Sci Mater Electron*. 2018;29:15486.

N.A. Narewadikar, R.S. Pedanekar, V.G. Parale et al.

34. Bharti B, Kumar S, Lee H-N, Kumar R. Formation of oxygen vacancies and Ti^{3+} state in TiO_2 thin film and enhanced optical properties by air plasma treatment. *Sci Rep*. 2016;6:32355.

35. Pérez-González M, Tomás SA, Santoyo-Salazar J, Morales-Luna M. Enhanced photocatalytic activity of TiO_2-ZnO thin films deposited by dc reactive magnetron sputtering. *Ceram Int*. 2017;43:8831.

36. Zhang H, Tan K, Zheng H, Gu Y, Zhang WF. Preparation, characterization and photocatalytic activity of TiO_2 codoped with yttrium and nitrogen. *Mater Chem Phys*. 2011;125:156.

37. Heo S, Sharma SK, Lee S, Lee Y, Kim C, Lee B, et al. Effects of Y contents on surface, structural, optical, and electrical properties for Y-doped ZnO thin films. *Thin Solid Films*. 2014;558:27.

38. Zhao B, Wang J, Li H, Wang H, Jia X, Su P. The influence of yttrium dopant on the properties of anatase nanoparticles and the performance of dye-sensitized solar cells. *Phys Chem Chem Phys*. 2015;17:14836.

39. Zhou J, Zhang Y, Zhao XS, Ray AK. Photodegradation of benzoic acid over metal-doped TiO_2. *Ind Eng Chem Res*. 2006;45:3503.

40. Mohd Said ND, Sahdan MZ, Nayan N, Saim H, Adriyanto F, Bakri AS, et al. Difference in structural and chemical properties of sol-gel spin coated Al doped TiO_2, Y doped TiO_2 and Gd doped TiO_2 based on trivalent dopants. *RSC Adv*. 2018;8:29686.

41. Choi J, Sudhagar P, Lakshmipathiraj P, Lee JW, Devadoss A, Lee S, et al. Three-dimensional Gd-doped TiO_2 fibrous photoelectrodes for efficient visible light-driven photocatalytic performance. *RSC Adv*. 2014;4:11750.

42. Ikram A, Sahai S, Rai S, Dass S, Shrivastav R, Satsangi VR. Enhanced photo-electrochemical conversion performance of ZnO quantum dots sensitized α-Fe_2O_3 thin films. *Int J Hydrogen Energy*. 2015;40:5583.

43. Qu X, Hou Y, Liu M, Shi L, Zhang M, Song H, et al. Yttrium doped TiO_2 porous film photoanode for dye-sensitized solar cells with enhanced photovoltaic performance. *Results Phys*. 2016;6:1051.

44. Deng X, Wang Y, Chen Y, Cui Z, Shi C. Yttrium-doped TiO_2 compact layers for efficient perovskite solar cells. *J Solid State Chem*. 2019;275:206.

45. Le Bahers T, Takanabe K. Combined theoretical and experimental characterizations of semiconductors for photoelectrocatalytic applications. *J Photochem Photobiol, C*. 2019;40:212.

46. Liu D, Tian R, Wang J, Nie E, Piao X, Li X, et al. Photoelectrocatalytic degradation of methylene blue using F doped TiO_2 photoelectrode under visible light irradiation. *Chemosphere*. 2017;185:574.

47. Kothavale VP, Patil TS, Patil PB, Bhosale CH. Photoelectrocatalytic degradation of Rhodamine B using N doped TiO_2 thin Films. *Mater Today Proc*. 2020;23:382.

48. Bhatia V, Dhir A. Transition metal doped TiO_2 mediated photocatalytic degradation of anti-inflammatory drug under solar irradiations. *J Environ Chem Eng*. 2016;4:1267.

49. Mishra PM, Kumar Sahoo S, Kumar Padhi D. Biomimetic synthesis of Ag/TiO_2 nanocomposites using a natural surfactant for effective degradation of an environmental pollutant. *SDRP-JESES*. 2020;5:44.

50. Theurich J, Bahnemann DW, Vogel R, Ehamed FE, Alhakimi G, Rajab I. Photocatalytic degradation of naphthalene and anthracene: GC-MS analysis of the degradation pathway. *Res Chem Intermed*. 1997;23:247.

51. Nzila A. Current status of the degradation of aliphatic and aromatic petroleum hydrocarbons by thermophilic microbes and future perspectives. *IJERPH*. 2018;15:2782.

52. Mohite VS, Mahadik MA, Kumbhar SS, Hunge YM, Kim JH, Moholkar AV, et al. Photoelectrocatalytic degradation of benzoic acid using Au doped TiO_2 thin films. *J Photochem Photobiol, B*. 2015;142:204.